Journal Pre-proofs

Load path sensitivity and multiaxial fatigue life prediction of metals under non-proportional loadings

Qing-Yun Deng, Shun-Peng Zhu, Xiaopeng Niu, Grzegorz Lesiuk, Wojciech Macek, Qingyuan Wang

PII: S0142-1123(22)00531-X
DOI: https://doi.org/10.1016/j.ijfatigue.2022.107281
Reference: JIJF 107281

To appear in: *International Journal of Fatigue*

Received Date: 3 August 2022
Revised Date: 14 September 2022
Accepted Date: 16 September 2022

Please cite this article as: Deng, Q-Y., Zhu, S-P., Niu, X., Lesiuk, G., Macek, W., Wang, Q., Load path sensitivity and multiaxial fatigue life prediction of metals under non-proportional loadings, *International Journal of Fatigue* (2022), doi: https://doi.org/10.1016/j.ijfatigue.2022.107281

Load path sensitivity and multiaxial fatigue life prediction of metals under non-proportional loadings

Qing-Yun Deng[1], **Shun-Peng Zhu**[1, 2, *], **Xiaopeng Niu**[1], **Grzegorz Lesiuk**[3], **Wojciech Macek**[4], **Qingyuan Wang**[5, 6, *]

[1]*School of Mechanical and Electrical Engineering, University of Electronic Science and Technology of China, Chengdu 611731, China*

[2]*Institute of Electronic and Information Engineering of UESTC in Guangdong, Dongguan 523808, China*

[3]*Wroclaw University of Science and Technology, Department of Mechanics, Materials Science and Biomedical Engineering, Smoluchowskiego 25, 50-370 Wroclaw, Poland*

[4]*Gdansk University of Technology, Faculty of Mechanical Engineering and Ship Technology, 11/12 Gabriela Narutowicza, Gdansk 80-233, Poland*

[5]*MOE Key Laboratory of Deep Earth Science and Engineering, College of Architecture and Environment, Sichuan University, Chengdu 610065, China*

[6]*Advanced Research Institute, Chengdu University, Chengdu 610106, China*

ABSTRACT: Engineering components often operate under complex loadings, in which the variable amplitude multiaxial stresses are raised by geometric discontinuities including holes, grooves, fillets and shoulders, etc. Besides, the non-proportional loading will lead to the rotation of maximum principal stress/strain and additional fatigue damage of structural elements in service. Consequently, the multiaxial and non-proportional loading have attracted increasing attentions. In this study, for distinguishing the effects of different load paths on fatigue life, a simple and applicable method to quantify the non-proportionality is defined, which comprehensively considers the influence of loadings on all material planes. A new equivalent strain damage parameter based on critical plane is proposed in this study. Specifically, to quantify the effect of non-proportional loading on fatigue damage, a non-proportional degree of loading on the generalized plane is developed. Coupling with the existing non-proportional coefficient, a novel fatigue damage parameter is derived by combining a non-proportional factor. Experimental data of 304 stainless steel, sintered porous iron and CuZn37 brass are utilized for model validation and comparison. Fatigue lives with different load paths are evaluated respectively. In comparison with the Fatemi-Socie (FS), Chen and Itoh models, proposed method more effectively

*Corresponding author.
E-mail address: zspeng2007@uestc.edu.cn (S.P. Zhu), wangqy@scu.edu.cn (Q.Y. Wang)

evaluate the multiaxial fatigue life of materials under non-proportional loadings.

Keywords: life prediction, non-proportionality**,** multiaxial fatigue, load path, critical plane

Nomenclature

Symbols			
A_{max}	Circle area with radius of maximum shear strain	α,β	Rotation angle
$A_{\theta max}$	Swept area of $\gamma_{\theta max}$	θ_c	Orientation angle of the critical plane
b,c	Fatigue strength/ductility exponent	Φ	Non-proportional factor
b_0,c_0	Shear fatigue strength/ductility exponent	ν_e	Elastic Poisson's ratio
C_{XY},C	Correlation coefficient	ν_{eff}	Effective Poisson's ratio
Cov	Covariance	σ,σ_θ,σ_p	Stress
E	Elastic modulus	σ_e	Standard deviation of errors
e_i,e	Error index	σ_n	Normal stress
f_{np}	Non-proportionality	σ_t	Ultimate tensile strength
G	Shear modulus	σ_y	Yield strength
K	Uniaxial strength coefficient	$\sigma_{n,max}$	Maximum normal stress
K'	Cyclic strength coefficient	σ'_f,ε'_f	Fatigue strength/ ductility coefficient
k	Material constant	σ_{NP}	Equivalent stress under out-of-phase loading
L,L',L_0	Cyclic strain path	σ_{IP}	Equivalent stress under in-phase loadings
l_{np}	Non-proportional coefficient	τ_s,τ_θ	Shear stress
N	Total number of specimens	τ'_f,γ'_f	Shear fatigue strength/ductility coefficient
N_f	Fatigue failure cycles	ε,ε_θ,ε_p	Strain
N_{ft}	Tested life	ε_n	Normal strain
N_{fp}	Predicted life	$\Delta\varepsilon_n$	Normal strain range
N_{f-NP}	Fatigue life under non-proportional loading	ε_1	Principal strain
N_{f-IP}	Fatigue life under proportional loading	$\Delta\gamma^p_{max}$	Plastic shear strain range
n'	Cyclic strain hardening exponent	γ_s,γ_θ	Shear strain
n	Uniaxial strain hardening exponent	$\Delta\gamma$	Shear strain range
r_{min},r_{max}	Minor and major semi-axis of MCE	*Abbreviations*	
Var	Variance	CPM	Critical plane methods
$X(t)$,$Y(t)$	Random variables	ECP	Energy-critical plane
x,y,z	Cartesian coordinate direction	FDP	Fatigue damage parameter
W_{NP}	Plastic work under 90°out-of-phase loading	FS	Fatemi-Socie model
W_0	Plastic work under uniaxial or proportional loading	MLP	Moment of load path
		MOI	Moment of inertia

λ_i	Eigenvalues	MCE	Minimum circumscribed ellipse
λ	Strain ratio	SFE	Stacking fault energy
ξ,φ	Phase angle		

1. Introduction

Due to the influences of geometric discontinuities (including holes, notches, fillets, chamfers, etc.) and complicated external loadings, engineering components are always subjected to multiaxial cyclic loadings [1–5], and multiaxial fatigue failure widely occurs at their weak regions. Unfortunately, owing to the influences of crack generation mechanism and real stress-strain state, multiaxial fatigue failure is more complex than that fatigue under uniaxial loadings [6–9]. In addition, the non-proportional loadings inevitably lead to rotation of principal stress direction and result in additional fatigue damage on the structural element [10, 11]. Hence, it is essential to develop robust and effective methods to estimate the fatigue life of real components under multiaxial and non-proportional loadings.

Based on the microscopic formation mechanisms and the modes of fatigue crack propagation, multiaxial fatigue life is estimated by the critical plane methods (CPM), where not only the stress and strain are considered, but also the direction of crack initiation plane is involved. Recently, increasing attempts have been performed for multiaxial fatigue assessment. Wu et al. [12,13] utilized the Wu–Hu–Song model to evaluate the multiaxial fatigue life together with test of aluminum alloy TC4. Zhu et al. [14–16] studied the normal/shear stress–strain response on the critical plane, and energy-critical plane (ECP) method was successfully applied to compressor turbine disc for estimating the fatigue life and achieved satisfactory results. In general, the existing CPM are classified into the stress-based parameter [17–19], strain-based parameter [20–22] and energy-based parameter [23–26]. Among them, the energy-based CPM are developed according to the concept of strain energy, which solves the controversies that energy is scalar but lack of explanation of crack initiation direction. The satisfactory estimations of multiaxial fatigue life under proportional (in-phase) loadings are presented through these above-mentioned methods, nevertheless, they are not applicable to fatigue assessment under multiaxial and non-proportional (out-of-phase) loadings which effects are overlooked.

In addition, multiaxial fatigue tests show that the fatigue life of the specimens would be reduced significantly by non-proportional loadings [27–29]. To take the effects of non-proportional loadings into account during multiaxial fatigue life assessment, a non-proportional factor Φ was introduced into the

multiaxial damage parameters applicable to proportional loadings [30]. It enhances to improve the applicability and accuracy of existing models. From this point of view, the current research mainly depends on the non-proportionality of loadings f_{np} and non-proportional coefficient l_{np} related to material.

$$\Phi = f(f_{np}, l_{np}) \tag{1}$$

where the non-proportional coefficient is usually thought to be related to the non-proportional additional hardening of materials. Kanazawa et al. [31] defined the non-proportional coefficient by the ratio of the equivalent stress under in-phase and 90° out-of- phase loading. Then Lu et al. [32], Shamsaei and Fatemi [33], Borodii and Shukaev [34], and Anes [35] also referred to the definition to assess the sensitivity of material to non-proportional loadings by using uniaxial and monotonic properties. Similarly, it has been found that the non-proportional loadings also significantly reduce the fatigue life of materials without obvious hardening. Borodii et al. [36] employed the ratio of two fatigue lives to characterize the non-proportional coefficient. f_{np} has been explained by abundant experiments and detailed discussions corresponding to above-mentioned methods can be seen in Section 2.2.

To differentiate different non-proportional loadings, existing feasible solutions are discussed in Section 2.3. Recent investigations indicate that the non-proportionality is directly with respect to the geometric characteristics of the load paths. Borodii et al. [36] pointed out that the load paths with larger enclosed area under the same equivalent stain show a greater non-proportional effect, where f_{np} in terms of the area ratio of the equivalent convex path to the circular load path is raised. Then the rotational inertia of the load paths was introduced to modified Borodii method by Zhong et al. [37]. In 5D deviatoric plastic strain space, Meggiolaro et al. [38–40] quantified the non-proportionality by using the moment of inertia (MOI) of the load paths. However, it is complicated for fatigue life prediction because equivalent path processing or intricate geometric operation is required. Besides, the non-proportional loadings usually result in the rotation of the principal axis of stresses or strains, f_{np} is also deemed to be related to the process of the principal axis rotation. In this process, the rotations of the shear stress (strain) or the normal stress (strain) vector on material plane determine the stress-strain response path. Kanazawa et al. [31, 41] determined the non-proportionality according to the ratio of shear strain amplitudes on different material planes. Itoh et al. [34] developed the integral form of f_{np} on basis of the maximum principal strain. The minimum normal strain range ratio was utilized to define the non-proportionality in Li et al. [42, 43]. Other forms of definitions can be found in Ref. [28, 38–40]. Since

the reliance of the calculations on stress-strain response path limits their applicability in engineering practice in which their methods seem to be intricate. Thus, an efficient method for discriminating non-proportional degree of different loadings is still lacking for engineering parts.

More effective multiaxial fatigue life prediction model suitable for general loading cases is expected for the field. In view of this, a new model based on CPM and non-proportional factor is proposed in this work. Firstly, due to the deficiencies of the existing critical-plane model that lack of considering crack initiation mechanism, a new fatigue damage parameter is raised to quantify the effects of normal stress and average stress. Then, a new quantification method of non-proportionality based on generalized material plane is proposed for considering the influences of non-proportional loading on fatigue damage. Combined with the existing non-proportional coefficient, the non-proportional factor is introduced to modify the proposed fatigue damage parameter, and yields to a new multiaxial fatigue damage model. The rationality and precision of the proposed approach are verified by the test results of type 304 stainless steel [47], sintered porous iron [48], and CuZn37 brass [49]. Furthermore, the FS [50], Chen [44] and Itoh [51, 52] models, suitable for non-proportional conditions, are applied to verify the predicted accuracy of the proposed model.

2. Revisiting some concepts of multiaxial fatigue

2.1 Analysis of multiaxial stress-strain state

Generally, engineering parts are often in complex stress-strain states, which can be well described by a vector (or matrix) including six stress–strain components, as shown in Fig. 1(a). For better studying the multiaxial mechanical behavior and failure mechanism, ASME code standard E2207 [13] designs smooth thin-walled tubular specimen for axial–torsional loading test. Theoretically, from the plane stress, the stress state can be shown in Fig. 1(b) and expressed as:

$$[\sigma]=\begin{bmatrix}\sigma_{xx} & \tau_{xy} & 0\\ \tau_{xy} & 0 & 0\\ 0 & 0 & 0\end{bmatrix} \qquad [\varepsilon]=\begin{bmatrix}\varepsilon_{xx} & \frac{1}{2}\gamma_{xy} & 0\\ \frac{1}{2}\gamma_{xy} & -\nu_{eff}\varepsilon_{xx} & 0\\ 0 & 0 & -\nu_{eff}\varepsilon_{xx}\end{bmatrix} \tag{2}$$

where $[\sigma]$ and $[\varepsilon]$ denote the stress and strain tensors, σ_{xx} and τ_{xy} denote the normal stress and shear stress, ε_{xx} and γ_{xy} denote the normal strain and shear strain, respectively. ν_{eff} is the effective Poisson's ratio and can be computed according to the literatures [53–55].

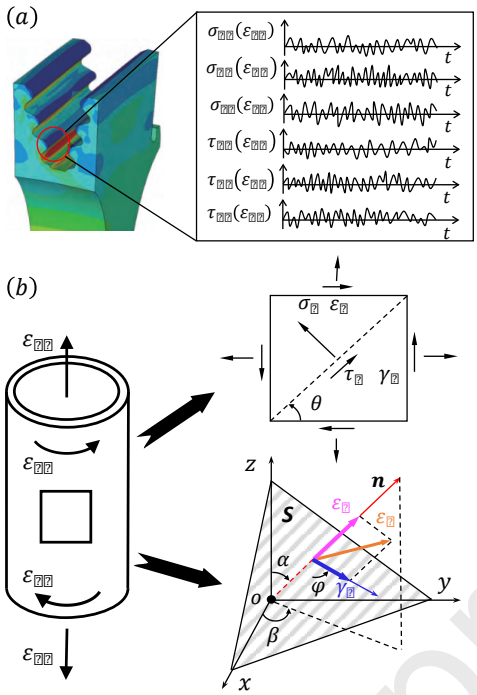

Fig. 1 Analysis of multiaxial stress-strain state

Through coordinate rotation, the normal and shear stresses (or strains) in all planes and directions can be expressed as follows:

$$\sigma_\theta = \frac{\sigma_{xx}}{2} + \frac{\sigma_{xx}}{2}\cos(2\theta) + \tau_{xy}\sin(2\theta) \tag{3}$$

$$\tau_\theta = \frac{\sigma_{xx}}{2}\sin(2\theta) - \tau_{xy}\cos(2\emptyset) \tag{4}$$

$$\varepsilon_\theta = (1-\nu_{eff})\frac{\varepsilon_{xx}}{2} + (1+\nu_{eff})\frac{\varepsilon_{xx}}{2}\cos(2\theta) + \frac{\gamma_{xy}}{2}\sin(2\theta) \tag{5}$$

$$\gamma_\theta = (1+\nu_{eff})\varepsilon_{xx}\sin(2\theta) - \gamma_{xy}\cos(2\theta) \tag{6}$$

where θ is the angle between the reference plane and the axial direction of the objects.

For strain-controlled tests, each strain is loaded with a sine wave curve, just as:

$$\varepsilon_{xx} = \frac{\Delta\varepsilon}{2}\sin(\omega t) \tag{7}$$

$$\gamma_{xy} = \lambda\frac{\Delta\varepsilon}{2}\sin(\omega t - \varphi) \tag{8}$$

$$\lambda = \frac{\Delta\gamma}{\Delta\varepsilon} \tag{9}$$

where $\Delta\varepsilon$ and $\Delta\gamma$ are normal and shear strain ranges, λ is the strain ratio and φ is the phase angle between the tensional and torsional strain.

According to the critical plane theory, crack initiation often starts from the plane with the maximum strain amplitude in the low cycle fatigue region. Taking ductile materials as an example, the parameters

on the critical plane with maximum shear strain amplitude are expressed as:

$$\frac{\partial \Delta\gamma}{\partial \theta} = 0 \tag{10}$$

$$\theta_c = \frac{1}{4}\tan^{-1}\left[\frac{2\lambda(1+\nu_{eff})\cos\varphi}{(1+\nu_{eff})^2-\lambda^2}\right] \tag{11}$$

$$\Delta\gamma_{max} = \Delta\varepsilon\left\{\left[\lambda\cos(2\theta_c)\cos(\varphi) - (1+\nu_{eff})\sin(2\theta_c)\right]^2 + \left[\lambda\cos(2\theta_c)\sin(\varphi)\right]^2\right\}^{\frac{1}{2}} \tag{12}$$

$$\Delta\varepsilon_n = \frac{\Delta\varepsilon}{2}\left\{\left[2(1+\nu_{eff})\cos(\theta_c)^2 - 2\nu_{eff} + \lambda\sin(2\theta_c)\cos(\varphi)\right]^2 + \left[\lambda\sin(2\theta_c)\sin(\varphi)\right]^2\right\}^{\frac{1}{2}} \tag{13}$$

where θ_c is the orientation angle of the critical plane, $\Delta\gamma_{max}$ is the maximum shear strain range and $\Delta\varepsilon_n$ is the normal strain range on the critical plane.

Because the stresses of real components cannot be simplified, Zhu et al. [7,14] give an algorithm to calculate the three-dimensional space of the critical plane. A material plane S defined by its unit normal vector $\boldsymbol{n}$ as shown in Fig. 1(b), which can be expressed through the angles α and β. While the second reference system can be expressed according to the following unit vector:

$$\boldsymbol{n} = \begin{bmatrix} n_x \\ n_y \\ n_z \end{bmatrix} = \begin{bmatrix} \sin\alpha\cos\beta \\ \sin\alpha\sin\beta \\ \cos\alpha \end{bmatrix} \tag{14}$$

The normal stress σ_n and normal strain ε_n of the S plane are calculated by:

$$\sigma_n = \boldsymbol{n}^T[\sigma]\boldsymbol{n} \qquad \varepsilon_n = \boldsymbol{n}^T[\varepsilon]\boldsymbol{n} \tag{15}$$

The shear stress τ_S and shear train γ_S on the S plane are expressed as:

$$\tau_S = |\boldsymbol{\sigma_p} - \boldsymbol{\sigma_n}| = \left|[\sigma]\boldsymbol{n} - (\boldsymbol{n}^T[\sigma]\boldsymbol{n})\boldsymbol{n}\right| \qquad \frac{\gamma_s}{2} = |\boldsymbol{\varepsilon_p} - \boldsymbol{\varepsilon_n}| = \left|[\varepsilon]\boldsymbol{n} - (\boldsymbol{n}^T[\varepsilon]\boldsymbol{n})\boldsymbol{n}\right|\boldsymbol{n} \tag{16}$$

Then combing with the definition of critical plane, the fatigue damage plane and the damage parameters are further obtained. More detailed descriptions are available in [6,14].

2.2 Non-proportionality coefficient

Facing different non-proportional loadings, materials often show different sensitivities. Taira et al. [56] firstly observed non-proportional hardening of materials in low cycle fatigue tests, where the fatigue behavior is obviously different from that under proportional loadings. Later, many scholars just like Lamba et al. [57] and Kanazawa et al. [31] noticed this phenomenon and tried to explain it. The rotation and staggering of the maximum shear plane under non-proportional loadings alter the crystalline slip plane, and it prevents the growth of stable dislocation and enhances hardening due to the slip planes intersection. To quantify the sensitivity of material microstructure to non-proportional loadings, the non-

proportionality coefficient l_{np} is introduced.

Kanazawa et al. [31] defined additional hardening by the ratio of stress amplitudes at region of large plastic strains in a fatigue cycle as:

$$l_{np} = \frac{\sigma_{NP}}{\sigma_{IP}} - 1 \tag{17}$$

where σ_{IP} and σ_{NP} are the equivalent stress under in-phase loading and out-of-phase loading, respectively, where σ_{NP} is 90 deg-out-of-phase loading (circular strain path in a $\gamma/\sqrt{3} - \varepsilon$ plot) and shows the maximum additional hardening in all the non-proportional load paths. Socie [58] took $l_{np} = 0.9$ for type 304 stainless steel. Doong et al. [59] considered l_{np} to zero for aluminum alloys existing little additional hardening.

Lu et al. [32] put forward a new non-proportional coefficient based on the ratio of plastic work of different paths at the same strain level:

$$l_{np} = \frac{W_{NP}}{W_0} - 1 \tag{18}$$

where W_0 is the plastic work under uniaxial or proportional loadings. W_{NP} is the plastic work under 90°out-of-phase loading (circular strain path for the same strain range). The dependence of non-proportional cyclic hardening on the material is explained based on the energy.

Considering the fatigue test cost and the convenience of engineering application, Shamsaei and Fatemi [33] raised the following empirical equation by connecting the non-proportionality coefficient l_{np} with the uniaxial monotonic and cyclic deformation characteristics of the objective material:

$$l_{np} = 1.6\left(\frac{K}{K'}\right)^2\left(\frac{\Delta\varepsilon}{2}\right)^{2(n-n')} - 3.8\left(\frac{K}{K'}\right)\left(\frac{\Delta\varepsilon}{2}\right)^{(n-n')} + 2.2 \tag{19}$$

where $\Delta\varepsilon$ denotes axial strain range. K and n denote uniaxial strength coefficient and strain hardening exponent, respectively. K' and n' denote cyclic strength coefficient and cyclic strain hardening exponent, respectively.

Borodii and Shukaev [34] explored in detail the relationships between the microphysical properties of metal materials and the microphysical parameters expressed by static properties and the sensitivity of cyclic strain hardening. On the one hand, the non-proportional hardening of the material is negatively correlated with the stacking fault energy (SFE). However, due to insufficient research, this satisfactory quantitative estimation has not been obtained yet. On the other hand, a clear semi-logarithmic linear relationship between the static characteristics and the non-proportional hardening level under cyclic loading was observed as:

$$m = \frac{\sigma_t}{\sigma_y} - 1 \tag{20}$$

$$\lg |l_{np}| = 0.705m - 1.22 \tag{21}$$

where m represents a dimensionless parameter. σ_t and σ_y represent the material ultimate tensile strength and yield strength, respectively. Similarly, a simple approximate non-proportional hardening model determined by static properties is established by Itoh et al. [60].

Besides, Borodii et al. [36] believed that the non-proportionality coefficient of materials could be derived conveniently from the S-N curves under proportional and non-proportional loadings. Consequently, Borodii and Shukaev [34] made the following recommendation for materials with high additional reinforcement:

$$l_{np} = \left| \frac{N_{f-NP}}{N_{f-IP}} - 1 \right| \tag{22}$$

where N_{f-NP} and N_{f-IP} are the fatigue lives under non-proportional tension-torsion (circular path) and proportional (tension-torsion) loading.

2.3 Non-proportionality of loadings

Because of the variety of non-proportional loadings, their influences on material fatigue damage not only relies on the material sensitivity, but also on the non-proportional loadings. Kanazawa et al. [31,41] firstly developed a rotation coefficient to define the non-proportionality of loadings by studying the plane of slip bands of l% Cr-Mo-V steel under axial and torsional non-proportional loadings:

$$f_{np} = \frac{\Delta\gamma_{45^\circ to\, S}}{\Delta\gamma_{max}} \tag{23}$$

where $\Delta\gamma_{max}$ is the maximum shear strain amplitude on the critical plane, $\Delta\gamma_{45^\circ to\, S}$ is shear strain range at 45° to the critical plane S. For sinusoidal loading, see Eq. (7-9), the non-proportionality f_{np} is described by the formula:

$$f_{np} = \sqrt{\frac{\lambda^2 + (1+\nu_{eff})^2 - \left(((1+\nu_{eff})^2 - \lambda^2)^2 + (2\lambda(1+\nu_{eff})\cos\varphi)^2\right)^{1/2}}{\lambda^2 + (1+\nu_{eff})^2 + \left(((1+\nu_{eff})^2 - \lambda^2)^2 + (2\lambda(1+\nu_{eff})\cos\varphi)^2\right)^{1/2}}} \tag{24}$$

Fatemi and Shamsaei et al. [50] pointed out that the additional hardening under non-proportional loadings could account for the maximum normal stress $\sigma_{n,max}$ on the maximum shear strain plane. Based on the relationship between the shear strain on the critical plane and the non-proportional load paths, De Freitas et al. [61] took into account the advantages of minimum circumscribed ellipse (MCE) approach and characterized the non-proportionality in an easy way:

$$f_{np} = \frac{r_{min}}{r_{max}} \tag{26}$$

where r_{min} and r_{max} are the minor and major semi-axis of MCE enclosing the shear strain path in Fig. 2, respectively.

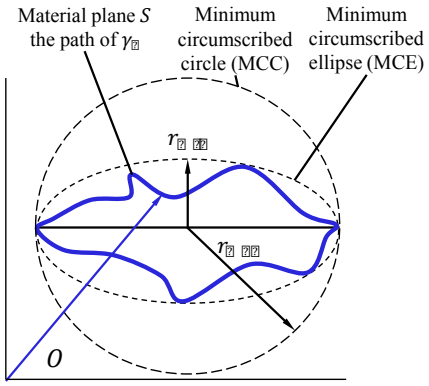

Fig. 2 The non-proportionality by MCE.

Through the study of the maximum shear strain in different directions during one cycle, Chen et al. [44] found that $\gamma_{\theta max} - \theta$ is a circle in the polar coordinate form as shown in Fig. 3 when $\lambda \approx 1.5$ and the phase angle $\varphi = 90^{\circ}$, which indicates that $\gamma_{\theta max}$ reaches the same maximum shear strain value in any direction θ. Combined with the dislocation theory, this non-proportional loading will lead to more active slip systems, which will affect the fatigue life of the material. Then, Chen et al. [44] advanced the following parameter to define the non-proportionality as:

$$f_{np} = 2\frac{A_{\theta max}}{A_{max}} - 1 \tag{27}$$

where A_{max} is the circle area with radius of maximum shear strain during one cycle, $A_{\theta max}$ is the swept area of $\gamma_{\theta max} - \theta$ polar coordinate space ($f_{np} = 0$ for proportional loading and $f_{np} = 1$ for $\varphi = 90^{\circ}$ and $\lambda \approx 1.5$). In general, the rank of non-proportionality is circular $>$ square $>$ cruciform $>$ proportional path, which consistent with the conclusions in [62].

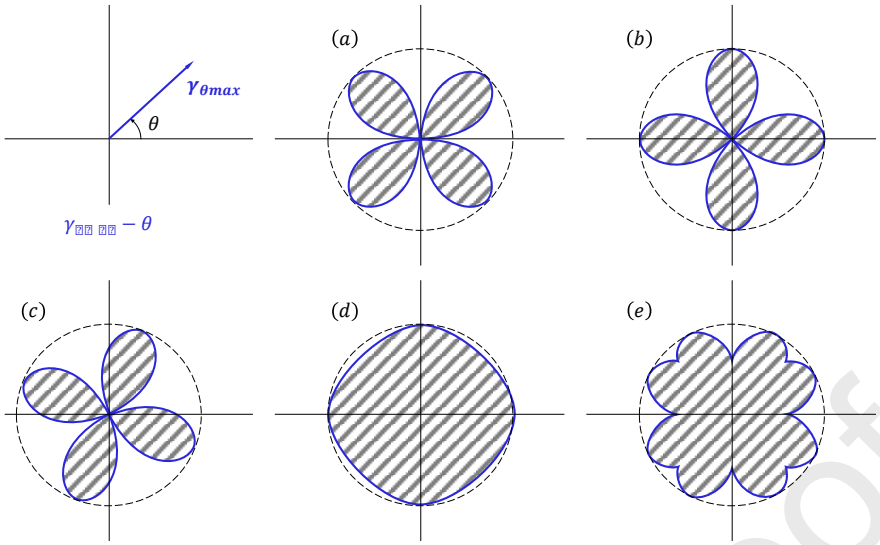

Fig. 3 $\gamma_{\theta max}$ versus θ relationships for different load paths, (a) Tension, (b) Torsion, (c) Proportional, (d) Circular, and (e) Square.

Itoh et al. [63] studied the low cycle fatigue life of Type 304 stainless steel under strain-controlled proportional and non-proportional load paths. Considering the impact of the principal strain direction on the non-proportional hardening of the material, the non-proportionality is characterized by:

$$f_{np} = \frac{1.57}{T\varepsilon_{1max}} \int_0^T (|\sin \xi(t)| \varepsilon_1(t)) dt \tag{28}$$

$$\varepsilon_1(t) = \begin{cases} |\varepsilon_1(t)| & \text{for } |\varepsilon_1(t)| > |\varepsilon_3(t)| \\ |\varepsilon_3(t)| & \text{for } |\varepsilon_3(t)| > |\varepsilon_1(t)| \end{cases} \tag{29}$$

where $\varepsilon_{1max} = max(\varepsilon_1(t))$ and $\xi(t)$ denote the angle between $\varepsilon_1(t)$ and ε_{1max}, which can be clearly described in Fig. 4. T denote the time for a loading cycle. For proportional loading, $\xi(t) \equiv 0$ and the value of f_{np} takes zero. Because of the variation of the direction and the complexity of the modified strain path, this integral form of non-proportionality is limited in practical application.

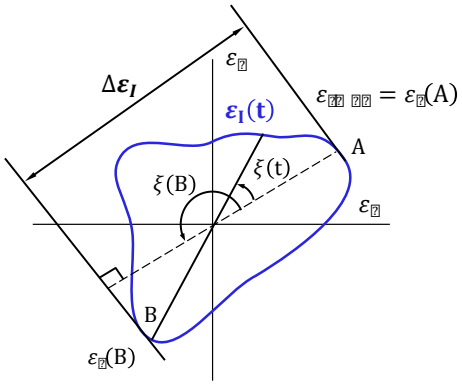

Fig. 4 Schematic graph of Itoh method.

The moment of inertia (MOI) model was firstly presented by Meggiolaro et al. [38–40], where the non-proportionality factor f_{np} is computed according to a transformed 5D deviatoric plastic strain space.

By obtaining the eigenvalues ($\lambda_1 \geq \lambda_2 \geq \lambda_3 \geq \lambda_4 \geq \lambda_5$) of the Rectangular MOI tensor with respect to the origin O, the value of non-proportionality was defined by the square root of the ratio between the two largest ones:

$$f_{np} = \sqrt{\frac{\lambda_2}{\lambda_1}} \tag{30}$$

Different from the above approaches by determining the non-proportionality based on the response parameters on the material plane, Borodii et al. [36] paid attention to the geometric characteristics of the biaxial cyclic load path:

$$f_{np} = \left(\frac{S_{L'}}{S_{L_0}}\right)^r \tag{31}$$

$$r = \left(1 - \frac{S_L}{S_{L_0}}\right)\frac{\oint_L d\boldsymbol{l}}{4\Delta\varepsilon_m} \tag{32}$$

where $S_L = \frac{1}{2}\oint_L \boldsymbol{e} \times d\boldsymbol{e}$, $S_{L'} = \frac{1}{2}\oint_{L'} \boldsymbol{e} \times d\boldsymbol{e}$ and $S_{L_0} = \frac{1}{2}\oint_{L_0} \boldsymbol{e} \times d\boldsymbol{e}$ are respectively the area of path L L' and L_0, depicted in Fig. 5(a), $\boldsymbol{e}$ and $d\boldsymbol{e}$ are the vectors of strain and strain increment, L is the cyclic strain path, L' is a convex equivalent path under any cyclic load path, L_0 is the circular path under the same maximum equivalent strain. Based on the second coordinate system of the above strain path, Zhong et al. [37] introduced the rotational inertia to modify the Borodii model, described in Fig. 5(b) and expressed as:

$$f_{np} = \left(\frac{\oint_{S_{L'}} y^2 dS_{L'}}{\oint_{S_L} y^2 dS_L}\right)^r \tag{33}$$

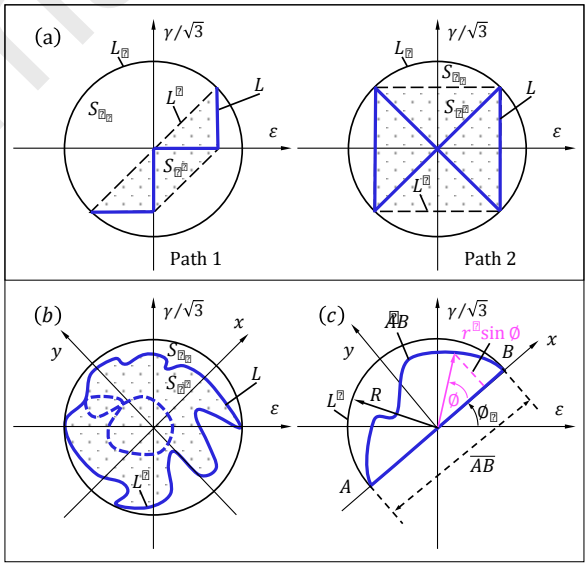

Fig. 5 Schematic graph about non-proportionality definitions of (a) Borodii model, (b) Zhong model, (c) Dong model.

Furthermore, Dong et al. [64, 65] put forward the moment of load path (MLP) model combined with a path-dependent cycle counting method, which assumed that the damage was directly related to each half cycle path. Utilizing the maximum non-proportional damage (semicircular load path), the non-proportionality factor f_{np} is expressed as:

$$f_{np} = \frac{\int_{\widetilde{AB}} r'|\sin\phi|ds'}{\int_{\overline{AB}} R|\sin\phi|ds} = \frac{\int_{\widetilde{AB}} r'|\sin\phi|ds'}{2R^2} \tag{34}$$

where $\widetilde{AB}$ is the path from A to B in a half cycle under non-proportional loadings, $\overline{AB}$ is the reference path from A to B, ϕ is the angular difference between r' and the reference axis, which can be represented in Fig. 5(c). Later, Liu et al. [66] modefied the MLP based on the viewpoint of inhomogeneous integral path and validated the present study. But owing to the difficulties to establish multiaxial counting algorithm and reference coordinates, such methods seems to be hardly implemeted.

2.4 Multiaxial fatigue life prediction under non-proportional loadings

Although numerous multiaxial fatigue damage parameters (FDP) based on stress, strain and energy have been developed [17–26], most of them are well adapted to specific loading cases, such as tension, torsion and proportional loadings. But the prediction effect of these parameters is not ideal, especially when the loading history is non-proportional. In this study, FS [50], Chen [44] and Itoh [51,52] models are employed to compare with the proposed model under non-proportional loadings.

2.4.1 FS model

The mean normal stress $\sigma_{n,m}$ have an significant impact on crack initiation and propagation, which is firstly observed by Socie et al. [58]. They illustrated the maximum normal stress on the basis of the model raised by Brown and Miller [67] to further consider the additional non-proportional hardening effect. FS model [50] was defined as:

$$FDP = \frac{\Delta\gamma_{max}}{2}\left(1 + k\frac{\sigma_{n,max}}{\sigma_y}\right) = \frac{\tau'_f}{G}(2N_f)^{b_0} + \gamma'_f(2N_f)^{c_0} \tag{35}$$

where τ'_f is the torsional fatigue strength coefficient, γ'_f is the torsional fatigue ductility coefficient, b_0 is the torsional fatigue strength exponent, c_0 is the torsional fatigue ductility exponent, N_f is the failure life, G is the shear modulus, $\sigma_{n,max}$ is the maximum shear stress on the plane of the maximum shear strain amplitude $\frac{\Delta\gamma_{max}}{2}$, k is material parameter fitted by the uniaxial data against the pure torsion data or constant [68]. Because of the simple and applicable mathematical form, FS model becomes one

of the most widely used models.

2.4.2 Chen model

Chen et al. [44] addressed that the plastic component dominates compared to the elastic component in the low cycle fatigue region, and the additional hardening effect of materials usually occurs after the plastic yield. Consequently, the impact of non-proportionality on the elastic component is neglected for low cycle fatigue, and plastic term of Coffin-Manson formula was modified as:

$$(1 + l_{np} f_{np})^{1/n'} \frac{\Delta\gamma^p_{max}}{2} = \gamma'_f (2N_f)^{c_0} \tag{36}$$

where l_{np} is computed by data fitting using Eq. (17), f_{np} is the distribution of maximum shear strain indirectly connecting the macroscopic effects of non-proportionality with the shear slip failure mechanism, expressed in Eq. (27), $\Delta\gamma^p_{max}$ is the range of plastic shear strain, n' is cyclic strain hardening exponent.

Considering the influences of the normal strain $\Delta\varepsilon_n$ vertical to the maximum shear strain plane on the fatigue crack growth rate, Brown and Miller [67] defined the equivalent damage parameter by using critical plane, where the maximum shear strain dominates the initiation and growth of the first stage crack while the normal strain component dominates the second stage. Since the BM model couldn't evaluate the non-proportional loading fatigue life, combined with Eq. (36), the effect of non-proportional additional hardening in the plastic region was introduced, and the modified critical plane damage parameter was expressed as:

$$FDP = \frac{\Delta\gamma_{max}}{2} + \frac{\Delta\varepsilon_n}{2} = \frac{\tau'_f}{G}(2N_f)^{b_0} + (1 + l_{np} f_{np})^{-1/n} \gamma'_f (2N_f)^{c_0} \tag{37}$$

2.4.3 Itoh model

According to numerous constant amplitude and multiaxial low cycle fatigue tests with different cyclic strain paths, Itoh et al. [63][69] found that the range of the maximum principal strain has apparent influences on the fatigue life. On the one hand, the principal stress/strain axis and the maximum shear plane of the material rotate under non-proportional cyclic loadings, which cause the transformation of slip bands and prevent the growth of stable dislocation. And then a significant reduction for fatigue life is performed by non-proportional additional hardening. The definition of loadings' non-proportionality is shown in Eq. (28), and the non-proportionality coefficient is defined by Eq. (17); On the other hand, their research also showed that the maximum principal strain range is well adapted to the proportional loadings, which possessing large error and non-conservative for the loadings with non-proportionality.

Therefore, Itoh et al. [51,52] take into account the influence of non-proportional additional hardening to estimate multiaxial fatigue by a non-proportional model, which is defined as:

$$FDP = \Delta\varepsilon_{\mathrm{I}}(1 + l_{np}f_{np}) = \frac{\sigma_f'}{E}(2N_f)^b + \varepsilon_f'(2N_f)^c \tag{37}$$

$$\Delta\varepsilon_{\mathrm{I}} = \max\left(\varepsilon_{\mathrm{I}max} - \cos\xi(t)\varepsilon_{\mathrm{I}}(t)\right) \tag{38}$$

where σ_f' and ε_f' denote the uniaxial fatigue strength coefficient and ductility coefficient, respectively; b and c denote the uniaxial fatigue strength exponent and ductility exponent, respectively; E is the elasticity modulus.

3. Proposed multiaxial fatigue life prediction model under non-proportional loadings

As mentioned in Section 2.1, the stress or strain on the critical plane has become the focus of attention for multiaxial fatigue models. Due to the complexity of loading conditions, that forms quantifying fatigue damage based on simplistic fatigue test results is less effective and the impact of non-proportionality loadings cannot be neglected. In this study, the fatigue test results of Type 304 stainless steel [47], sintered porous iron [48], and CuZn37 brass [49] under different load paths are investigated. As depicted in Fig. 6, all the cyclic load paths under tension, torsion, proportional and non-proportional loadings are presented. Particularly, in comparison with proportional loading, the fatigue lives of non-proportional load paths are lower with the same equivalent strain amplitude $\Delta\varepsilon_{eq,a}\sqrt{{\varepsilon_{xx}}^2 + {\gamma_{xy}}^2/3}$, which are presented in Fig. 7. Therefore, the damage parameters must be taken into account due to the influences of non-proportional loading on fatigue life.

Consequently, a more applicable equivalent damage parameter embraced the novel material state parameter and the parameter corresponding to non-proportional loading is raised to conduct multiaxial fatigue life prediction under non-proportional loadings as:

$$FDP = F(f_{np}, l_{np}, \sigma, \varepsilon) \tag{39}$$

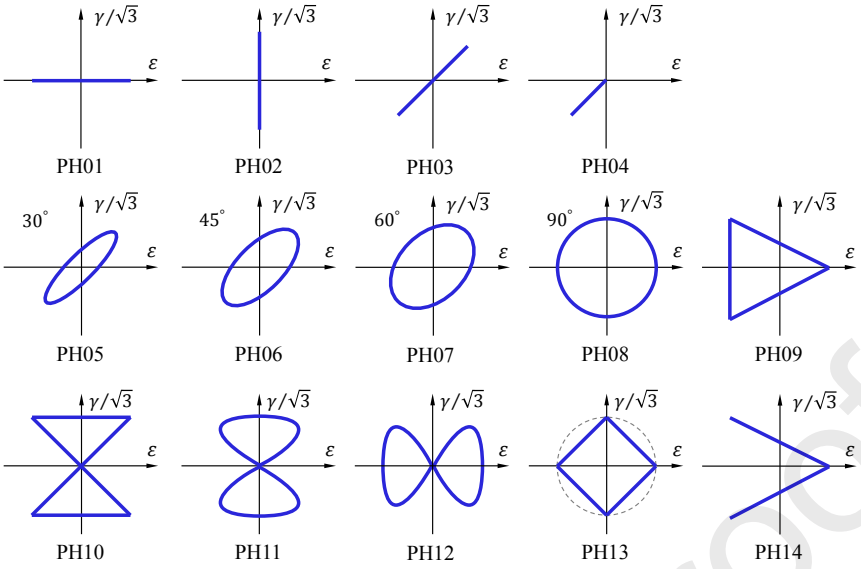

Fig. 6 Different proportional and non-proportional load paths [47–49].

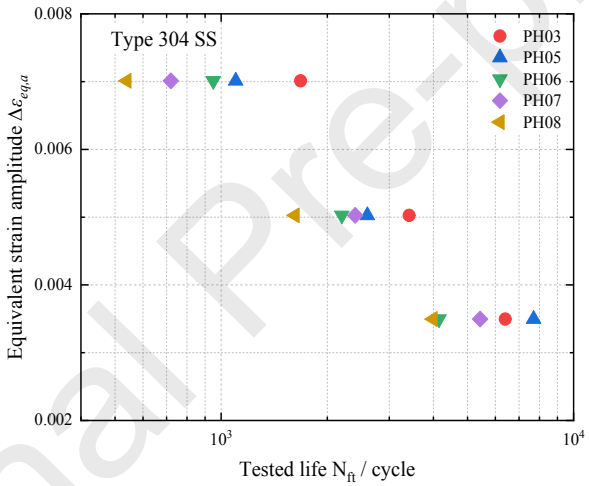

(a)

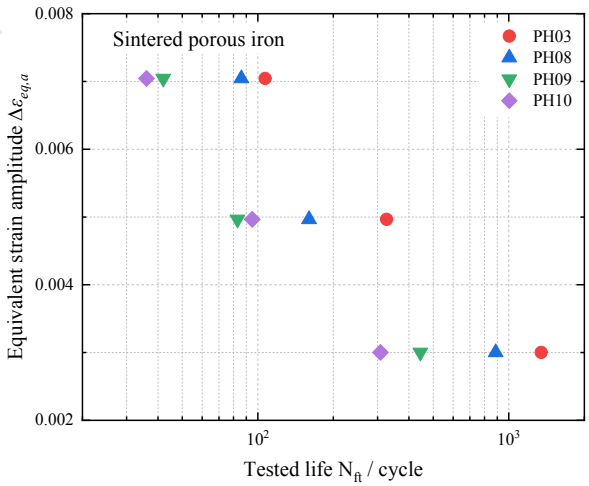

(b)

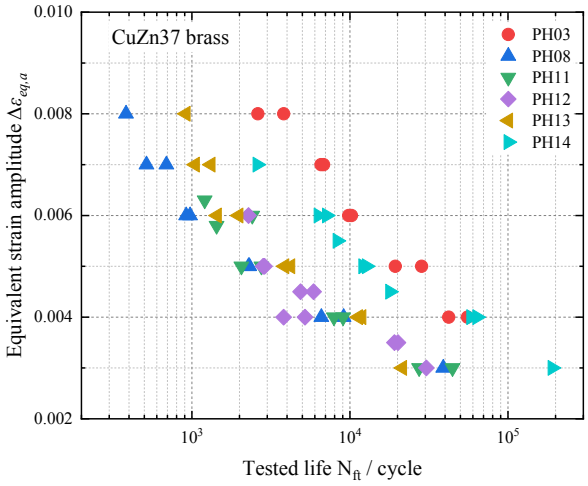

(c)

Fig. 7 Equivalent strain amplitude versus tested lives under different load paths for (a) Type 304 stainless steel, (b) Sintered porous iron, (c) CuZn37 brass.

3.1 New non-proportionality of loadings

In the field of signal processing, the correlation between time signals is usually elaborated by correlation coefficient, known as Pearson correlation coefficient [70]. For instance, $X(t)$ and $Y(t)$ are two independent random variables and the correlation coefficient C_{XY} can be evaluated as:

$$C_{XY} = \frac{Cov(X(t),Y(t))}{\sqrt{Var(X(t))Var(Y(t))}} \tag{40}$$

where the covariance $Cov(X(t),Y(t))$, the variance $Var(X(t))$, $Var(Y(t))$ and the mean value $\overline{X}$, $\overline{Y}$ are computed by:

$$Cov(X(t),Y(t)) = \frac{1}{T}\int_0^T (X(t)-\overline{X})(Y(t)-\overline{Y})dt \tag{41}$$

$$Var(X(t)) = \frac{1}{T}\int_0^T (X(t)-\overline{X})^2 dt \qquad Var(Y(t)) = \frac{1}{T}\int_0^T (Y(t)-\overline{Y})^2 dt \tag{42}$$

$$\overline{X} = \frac{1}{T}\int_0^T X(t)dt \qquad \overline{Y} = \frac{1}{T}\int_0^T Y(t)dt \tag{43}$$

C_{XY} provides a numerical measure of variable correlation, whose range is [-1,1]. In particular, $C_{XY} = \pm 1$ indicates that the variables have proportional correlation and $C_{XY} = 0$ indicates that the variables are fully uncorrelated.

For the loading case like Eqs. (6-7), the correlation coefficient $C(\varepsilon_{xx}, \gamma_{xy}) = \cos\varphi$ can be introduced to quantify the proportionality of the loadings. Since the phase angle $\varphi = 0^\circ$, $C(\varepsilon_{xx}, \gamma_{xy}) = 1$ is with respect to the proportional loading, when the phase angle $\varphi = 90^\circ$, $C(\varepsilon_{xx}, \gamma_{xy}) = 0$ is with

respect to the non-proportional loading. The correlation coefficient is opposite to the non-proportionality.

As is shown in Fig. 8, the strain components ε_n and γ_s are of great importance on the material plane, which affect crack initiation and the formation of slip bands. In view of the correlation theory, a simple and effective form is defined to quantify the proportionality of the strain components as follows:

$$f_p = [C(\varepsilon_n, \gamma_s)]^2 \tag{44}$$

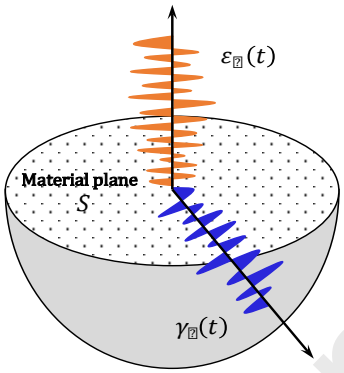

Fig. 8 ε_n and γ_s on the material plane.

Considering the rotation of the maximum principal stress or shear strain plane in a loading cycle, the non-proportionality of loadings on different planes characterized by two angle transformation as shown in Fig. 1(b) should be taken into account in the effects on fatigue damage. Thus, the new generalized non-proportionality is expressed as:

$$f_{np} = 1 - \frac{1}{2\pi^2}\int_0^{\pi}\int_0^{2\pi} f_p \, d\beta \, d\alpha = 1 - \frac{1}{2\pi^2}\int_0^{\pi}\int_0^{2\pi} [C(\varepsilon_n, \gamma_s)]^2 \, d\beta \, d\alpha \tag{45}$$

In this work, α and β are discretized to search the critical plane and setting the angle increment to 1° which is supposed to be an economical and effective option. Eq. (45) can be modified as:

$$f_{np} = 1 - \frac{1}{181 * 361}\sum_{i=1}^{181}\sum_{j=1}^{361}[C(\varepsilon_n, \gamma_s)]^2 \tag{46}$$

By this way, the integral calculation using complex strain paths is simplified and different non-proportional paths are also distinguished from the perspective of signal processing. Furthermore, Table 1 shows the non-proportionality calculation results of Type 304 stainless steel under seven load paths. f_{np} under tension, torsion and proportional loadings are calculated as zero. The value of non-proportionality gradually increases along with the path change from PH05 to PH08 (phase angles are 30°, 45°, 60° and 90° respectively). Especially, the calculated value of the proposed method under the path of PH08 is inconsistent with the results of Chen and Itoh model, because the proposed method comprehensively considers the non-proportional degree of loadings on all material planes.

Table 1 Results for calculating the non-proportionality of Type 304 stainless steel when $\lambda = 1.5$.

Strain paths	PH01	PH01	PH03	PH05	PH06	PH07	PH08
Proposed	0	0	0	0.38	0.55	0.68	0.80
Chen	0	0	0	0.07	0.18	0.34	1
Itoh	0	0	0	0.59	0.73	0.85	1

3.2 Proposed model

As aforementioned, the damage parameters on the critical plane have become a research consensus [17–26] Note from [50] that the shear strain amplitude is the most major factor of fatigue failure and the maximum normal stress on the maximum shear plane is thought to be the secondary one, which has also been proved in [71]. In order to match the shear form of Coffin-Manson equation, the equivalent damage parameter is demanded. Nevertheless, how to normalize the influence of normal stress is a matter that must be discussed.

In FS model, $\frac{\sigma_{n,max}}{\sigma_y}$ is the first attempt to normalize the influence of normal stress with material constant. Nevertheless, the introduction of additional material parameter k results in controversial discussions on the model. Wu et al. [13] thought of k as an experimental coefficient, whereas Karolczuk et al. [72] regarded k as the function of the axial and shear fatigue characteristics. The form of $k(N_f)$ expressed as follows has never been applied in calculations of the fatigue lives, which requires the application of an adequate number of fatigue failure data:

$$k = \left[\frac{\frac{\tau_f'}{G}(2N_f)^{b_0} + \gamma_f'(2N_f)^{c_0}}{(1+\nu_e)\frac{\sigma_f'}{E}(2N_f)^{b} + (1+\nu_p)\varepsilon_f'(2N_f)^{c}} - 1\right]\frac{2\sigma_y}{\sigma_f'(2N_f)^{b}} \tag{47}$$

where ν_e and ν_p are the elastic and plastic Poisson's ratios, respectively. Other CPM [13,16,17,20] also inevitably introduced additional material parameter to measure the impact of normal and shear parameters on fatigue life.

Therefore, Xu et al. [15] took $\frac{\sigma_y}{\sigma_f'}$ as an approximation of k to simplify the correction term as $\frac{\sigma_{n,max}}{\sigma_f'}$ by considering the influences of normal work on the maximum virtual shear strain energy E_{Smax} plane. Thus, Xu model was given as:

$$FDP = E_{Smax}\left(1 + \frac{\sigma_{n,max}}{\sigma_f'}\right) = f(N_f) \tag{48}$$

In a modified generalized strain amplitude model, Shang et al. [3] advanced the equivalent stress correction factor $\left(\frac{\tau_{max}}{\tau_f'}+\frac{\sigma_{n,max}}{\sqrt{3}\sigma_f'}\right)$ to characterize the influences of shear and normal stress, which are neglected for the strain-based critical plane model. Besides, in order to distinguish the difference between the effects of normal strain and shear strain on the critical plan, Yu et al. [68] normalized the normal strain to reflect the influences of normal strain on crack propagation by introducing the cyclic yield stress, and Yu model was given as:

$$FDP=\frac{\tau_{max}\Delta\gamma_{max}}{\tau_f'\quad 2}+\frac{2\sigma_{n,max}\Delta\varepsilon_n}{\sigma_f'+\sigma_y\ 2}=f(N_f) \tag{49}$$

Viewing the advantages of the above models, the material constitutive parameters σ_y and fatigue characteristic parameters σ_f' are comprehensively considered to modify the normal stress parameters. Hence, the strain model modified by the influence of normal stress parameters by $\frac{2\sigma_{n,max}}{\sigma_f'+\sigma_y}$ can be used for fatigue damage parameter under proportional loadings as:

$$FDP_{IP}=\frac{\Delta\gamma_{max}}{2}\left(1+\frac{2\sigma_{n,max}}{\sigma_f'+\sigma_y}\right)=\frac{\tau_f'}{G}(2N_f)^{b_0}+\gamma_f'(2N_f)^{c_0} \tag{50}$$

To consider the effect of non-proportional loading, in company with the non-proportional coefficient in Eq. (17) and new non-proportionality Eq. (46), the non-proportional correction factor Φ is given as:

$$\Phi=f(f_{np},l_{np})=1+l_{np}f_{np} \tag{51}$$

Then the equivalent strain parameter based on the critical plane can be modified as:

$$FDP=\Phi FDP_{IP}=(1+l_{np}f_{np})\frac{\Delta\gamma_{max}}{2}\left(1+\frac{2\sigma_{n,max}}{\sigma_f'+\sigma_y}\right)=\frac{\tau_f'}{G}(2N_f)^{b_0}+\gamma_f'(2N_f)^{c_0} \tag{52}$$

Noting that Eq. (52) will be simplified as Eq. (50) when the material is insensitive to non-proportional loading ($l_{np}=0$) or the non-proportionality of loading is zero ($f_{np}=0$). The damage parameter in Eq. (52) not only considers the influence of normal stress effect but also reflects the generalized influence of non-proportional loading on multiaxial fatigue damage. In conclusion, a multiaxial fatigue evaluation procedure considering non-proportional load paths is presented in Fig. 9, which provides a systematic solution for engineering researchers.

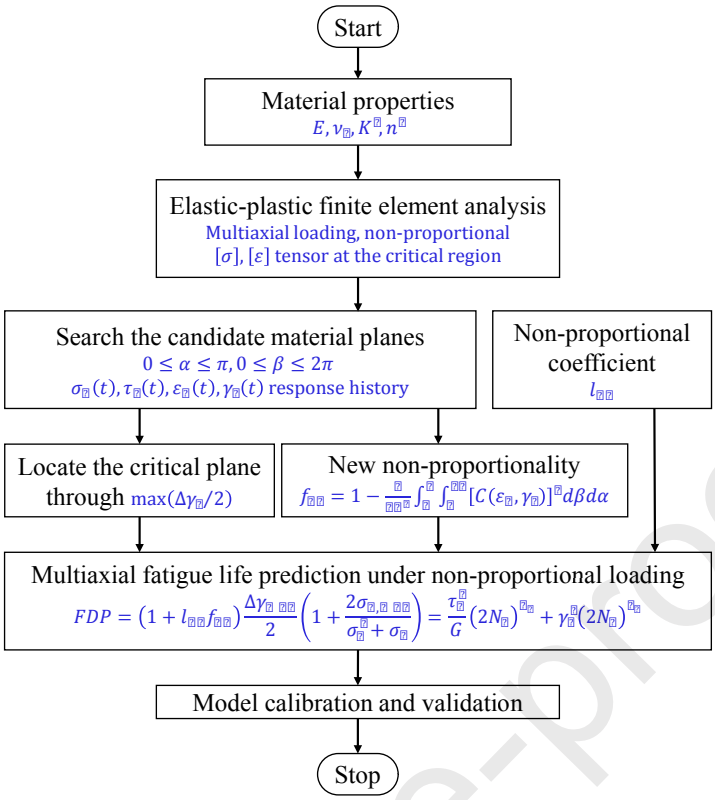

Fig. 9 Proposed procedure for multiaxial fatigue life prediction

4. Experimental verification and comparison

In order to estimate the prediction capability of the above-mentioned prediction models under multiaxial and non-proportional loadings, three kinds of experimental data of Type 304 stainless steel [47], sintered porous iron [48], and CuZn37 brass [49] are employed, and the material properties are summarized in Table 2. All the cyclic load paths are presented in Fig. 6. It is noteworthy that all fatigue tests are conducted using servo-controlled machines under strain-controlled axial–torsional deformation. These test signals are obtained by sinusoidal, triangular, trapezoidal waveforms, and most of them are fully reversed loadings except for PH04. There is thin-walled tubular specimen with reference to ASTM E2207 [73], which has been depicted in Fig. 10. The outer diameter D, inner diameter d and the gage length L of three type of specimens are given in Table 2, respectively.

Table 2 Material properties and specimen geometries of the three materials.

Materials	**Type 304 stainless steel** [47]	**Sintered porous iron** [48]	**CuZn37 brass** [49]
Monotonic properties			
E/GPa	167.5	162	132

G/GPa	56	62.3	49.6
σ_y/MPa	325	126.6	138
ν_e	0.3	0.3	0.33
Fatigue properties for axial or torsion			
σ'_f/MPa	691	289	301.7
ε'_f	0.101	0.047	0.069
b	-0.169	-0.074	-0.2599
c	-0.377	-0.406	-0.26
τ'_f/MPa	1137	166.85	183.9
γ'_f	1.055	0.3588	0.9612
b_0	-0.215	-0.0754	-0.012
c_0	-0.566	-0.5049	-0.4702
K'/MPa	1932	466.5	819
n'	0.449	0.172	0.2142
k	1.3	1	0.69
l_{np}	0.9	0.45	0.4
Specimen geometries			
D/mm	10	12	7
d/mm	13	16	10
L/mm	12.5	28	26

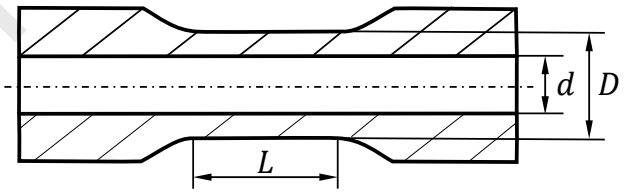

Fig. 10 Geometry of the thin-walled tubular specimen.

For illustrating the advantages of the proposed model compared with other models, an error index e is employed to estimate the deviation between the predicted and tested results:

$$e = \log_{10}(N_{fp}) - \log_{10}(N_{ft}) \tag{53}$$

where e_i presents the criterion prediction error, N_{fp} and N_{ft} denote the estimated life and experimental life.

Besides, the dispersion and overall deviation of prediction error are quantified by the normal distribution, which can be well described in the error box-plot:

$$\bar{e} = \frac{1}{N}\sum_{i=1}^{N} e_i \qquad f(e) = \frac{1}{\sqrt{2\pi}\sigma_e} exp\left(-\frac{(e-\bar{e})^2}{2{\sigma_e}^2}\right) \tag{54}$$

where $\bar{e}$ is the mean absolute deviation, N is the number of specimens, σ_e is the standard deviation of the error.

4.1 Type 304 stainless steel

Type 304 stainless steel were tested under PH01-03 and PH05-08 load paths in Fig. 6. Among of them, the non-proportional loadings include 30°, 45°, 60° and 90° out-of-phase. As shown in Fig. 11, tested and predicted lives derived via the proposed model and three conventional models are compared, where the solid line represents that the predicted results have a good agreement with tested data, the red dashed line and blue dashed line represent the life scatter factor of 2 and 3, respectively. The proposed model provides better agreement with the experimental data, all the points fall in the ± 2 bands, whereas many prediction points by FS, Chen and Itoh models fall out of even the life scatter factor of 3. As shown in Fig. 12, the average value of prediction errors is close to 0 and the proposed model shows the good robustness seeing the lowest standard deviation. The mean prediction error and the standard deviation of the proposed model are 34% and 41.6% lower than that of the FS model with better results than other two models, respectively.

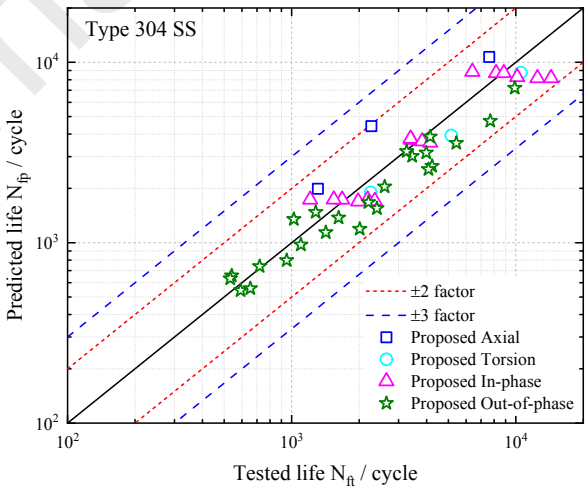

(a)

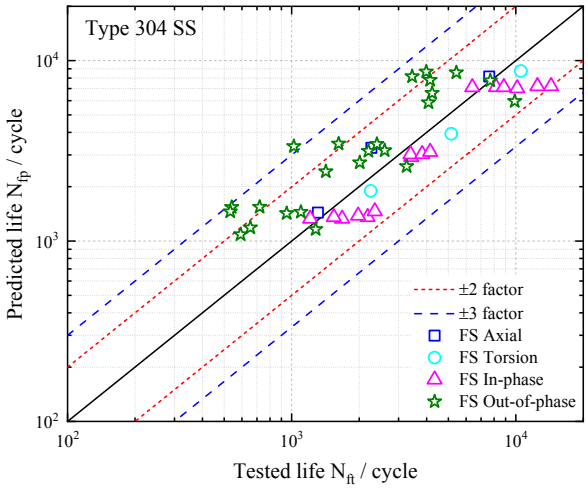

(b)

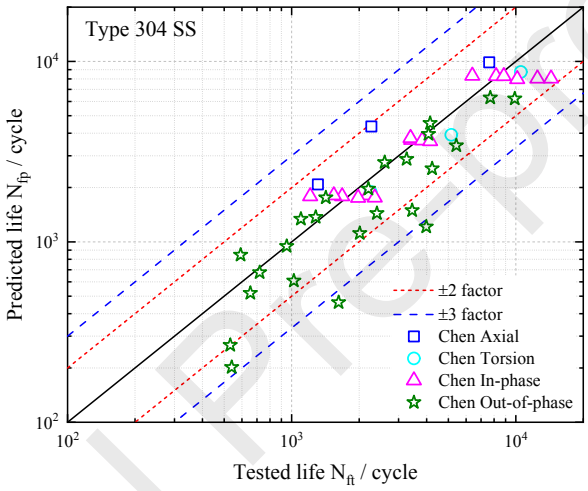

(c)

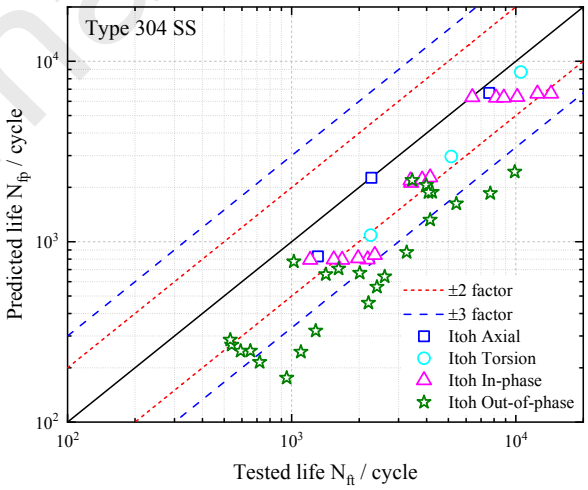

(d)

Fig. 11 Comparison between predicted and tested lives for Type 304 stainless steel by the (a) Proposed model, (b) FS model, (c) Chen model, and (d) Itoh model.

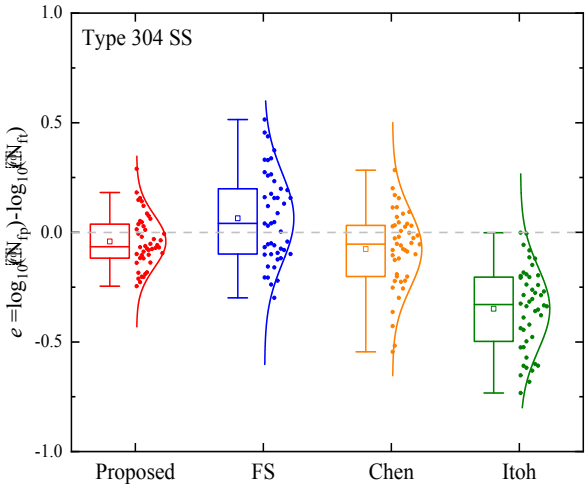

Fig. 12 Box plot of model prediction errors for Type 304 stainless steel.

4.2 Sintered porous iron

Sintered porous iron [48] were tested under torsion, two in-phase and three kind of non-propositional loadings, PH02-04 and PH08-10 depicted in Fig. 6. For torsion and in-phase loading tests, the proposed model and FS model present similar good prediction results according to Fig. 13. Noted that the proposed model submits better prediction results within the life scatter factor of 2 under various non-propositional loadings, whereas FS and Chen models have poor performance. Similarly, the box plot of model prediction errors in Fig. 14 makes clear that the proposed model yields the most accurate predictions, in which prediction error and the standard deviation are reduced by 82% and 38.7% than that of FS model, respectively. In addition, it also reflects that the maximum principal strain range of Itoh model is not appropriate for the sintered porous iron as a result of extreme deviation between the prediction results and the tested data under torsion and in phase loadings.

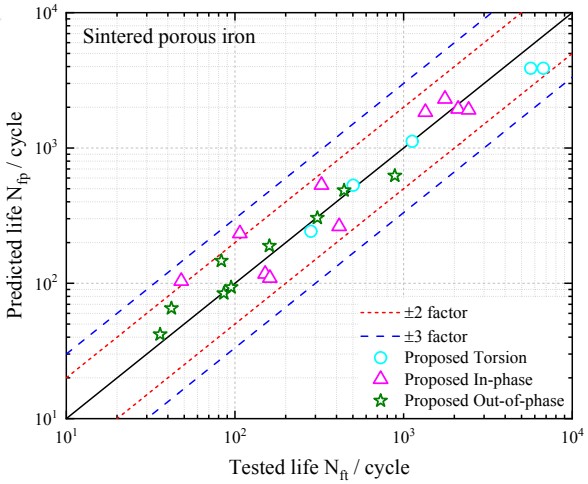

(a)

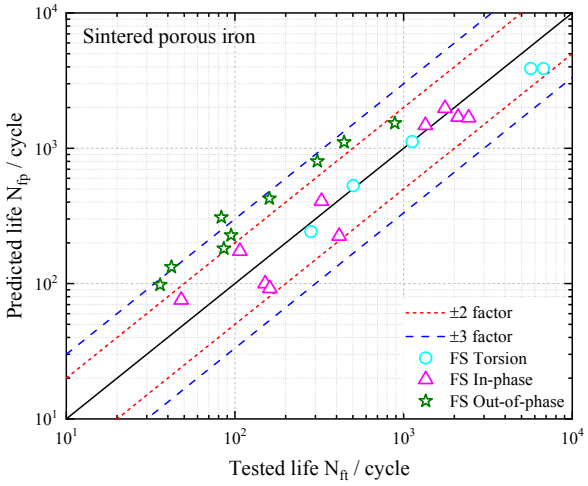

(b)

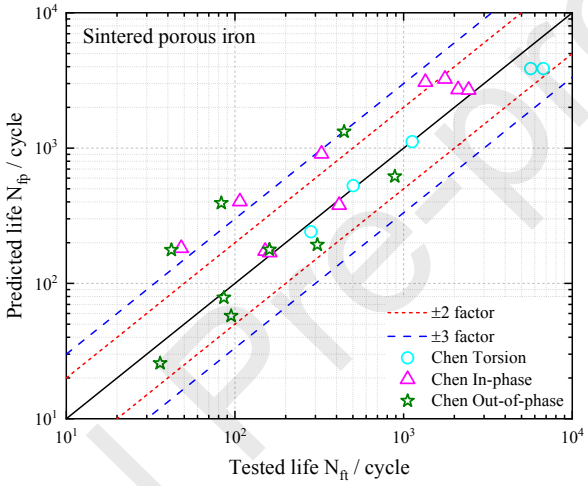

(c)

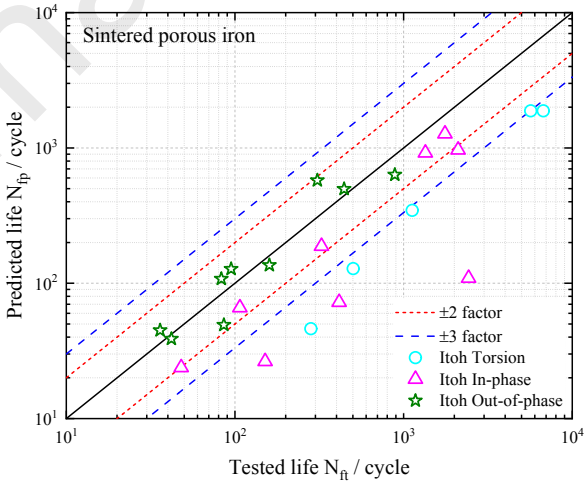

(d)

Fig. 13 Comparison between predicted and tested lives for Sintered porous iron by the (a) Proposed model, (b) FS model, (c) Chen model, and (d) Itoh model.

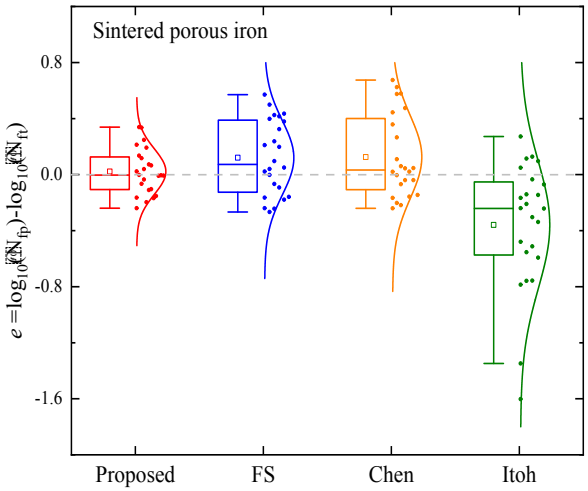

Fig. 14 Box plot of model prediction errors for Sintered porous iron.

4.3 CuZn37 brass

Several groups of multiaxial tests [49] were performed under load paths PH01-03, PH08 and PH11-14 in Fig. 6. As depicted in Fig. 15, all the predicted lives by the proposed model shown the better robustness than other three classic multiaxial fatigue models, most of which locate in the ± 2 error bands except 5 of 79 prediction points. For the above five kinds of non-proportional loadings, the prediction results of Chen and Itoh models are highly scattered and several prediction points are outside the life scatter factor of 2. Moreover, Fig. 16 indicates that the proposed model has the better prediction results compared to other models due to the lower prediction errors and standard deviation. Particularly, the mean prediction error is reduced by 9%, and the standard deviation is reduced by 13.8% compared with the FS model, and it is significantly better than the Chen and Itoh models.

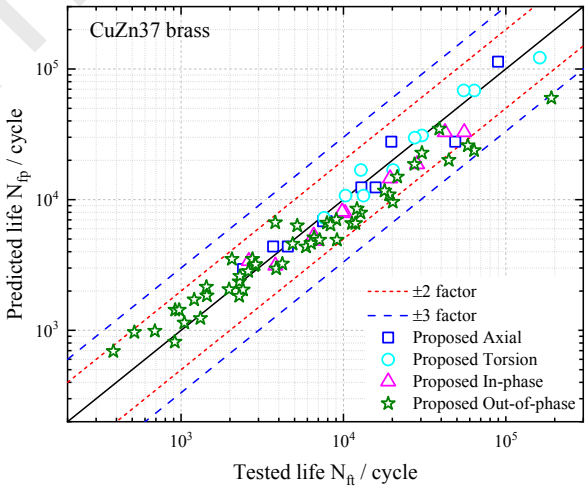

(a)

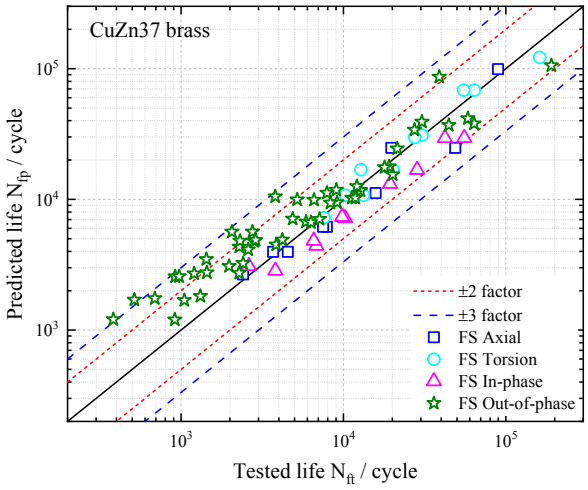

(b)

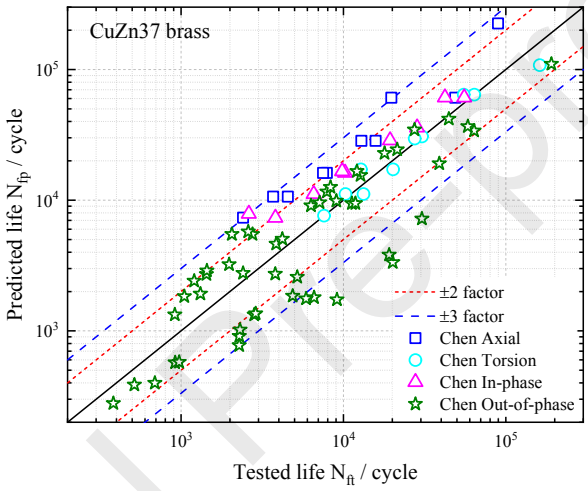

(c)

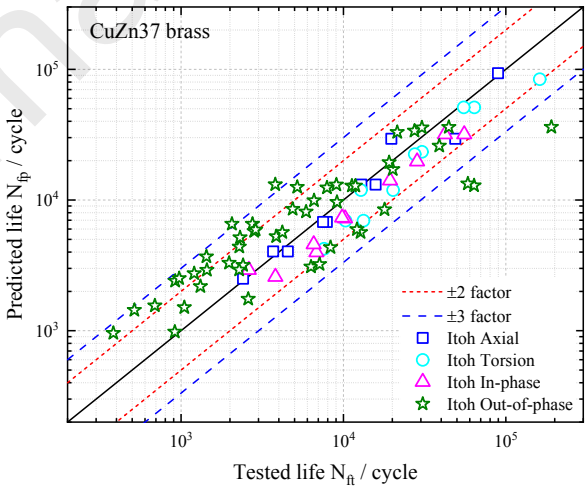

(d)

Fig. 15 Comparison between predicted and tested lives for CuZn37 brass by the (a) Proposed model, (b) FS model, (c) Chen model, and (d) Itoh model.

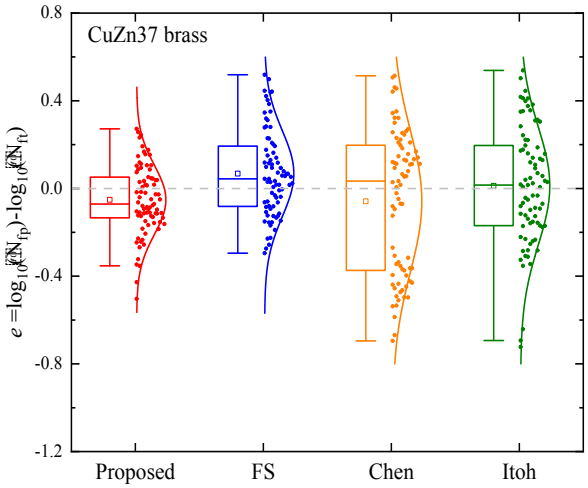

Fig. 16 Box plot of model prediction errors for CuZn37 brass.

According to the prediction results of several materials, it indicates that the proposed multiaxial fatigue model in this work is superior to the other three methods under different load paths. Firstly, the model considers the non-proportionality of loadings on the generalized plane and gives a simple and efficient solution. On the other hand, the critical plane damage parameters are redefined and the correction of additional material parameters is eliminated. Although more engineering material data are needed to verify, these revisions are conducive to the further development and application of multiaxial fatigue model.

5. Conclusion

In this work, a novel multiaxial fatigue model combining the critical plane theory with a new non-proportional influence factor is proposed for life prediction under various non-proportional load paths. The main conclusions are summarized as followed:

(1) The existing multiaxial experimental results indicate that the fatigue life not only relies on the equivalent strain amplitude, but also on the non-proportionality of loading for materials sensitive to non-proportional hardening. Therefore, the non-proportionality of loadings and multiaxial stress state should be paid more attention to.

(2) Through a comparative study on the non-proportionality of loadings, a simple definition of non-proportional degree on generalized plane is derived, which provides similar calculated value of f_{np} with Chen and Itoh models. Combined with the non-proportional coefficient of materials l_{np}, a new non-proportional correction factor Φ is raised.

(3) The effect of normal stress on the critical plane is considered by introducing a correction factor

without additional material parameters. Based on FDP under proportional loading and new non-proportional factor Φ, a new multiaxial model applicable to different non-proportional load paths is proposed for fatigue life prediction of materials.

(4) Comparing to FS model, the proposed model provides better agreement with the tested data for the three materials, which are almost within the error factor of 2, whereas Chen and Itoh models perform worse. The proposed model performs a better capability to predict fatigue life under multiaxial and non-proportional loadings, wherein the influences of normal stress are taken into account.

Acknowledgement

Financial support of the National Natural Science Foundation of China (No. 12232004 and 11972110), Sichuan Science and Technology Program (No. 2022JDJQ0024), and Guangdong Basic and Applied Basic Research Foundation (No. 2021B1515140030) are acknowledged.

References

[1] Li XK, Chen S, Zhu SP, Liao D, Gao JW. Probabilistic fatigue life prediction of notched components using strain energy density approach. Eng Fail Anal 2021;124:105375.

[2] Liu X, Wu Q, Su S, Wang Y. Evaluation and prediction of material fatigue characteristics under impact loads: review and prospects. Int J Struct Integr 2022;13(2): 251-277.

[3] Xue L, Shang DG, Li DH, Li LJ, Liu XD, Chen H. Equivalent energy-based critical plane fatigue damage parameter for multiaxial LCF under variable amplitude loading. Int J Fatigue 2020;131:105350.

[4] Ronchei C, Carpinteri A, Scorza D, Zanichelli A, Vantadori S. The RED criterion for fatigue life assessment of metals under non-proportional loading. Int J Fatigue 2022;107080.

[5] Zhao B, Xie L, Wang L, Hu Z, Zhou S, Bai X. A new multiaxial fatigue life prediction model for aircraft aluminum alloy. Int J Fatigue 2021;143:105993.

[6] Deng QY, Zhu SP, He JC, Li XK, Carpinteri A. Multiaxial fatigue under variable amplitude loadings: review and solutions. Int J Struct Integr 2022;13(3):349–93.

[7] Liao D, Zhu SP, Qian G. Multiaxial fatigue analysis of notched components using combined critical plane and critical distance approach. Int J Mech Sci 2019;160:38–50.

[8] Branco R, Costa JD, Borrego LP, Berto F, Razavi SMJ, Macek W. Comparison of different one-

parameter damage laws and local stress-strain approaches in multiaxial fatigue life assessment of notched components. Int J Fatigue 2021;151:106405.

[9] Marciniak Z, Rozumek D, Macha E. Verification of fatigue critical plane position according to variance and damage accumulation methods under multiaxial loading. Int J Fatigue 2014;58:84–93.

[10] Pejkowski Ł. On the material's sensitivity to non-proportionality of fatigue loading. Arch Civ Mech Eng 2017;17(3):711–27.

[11] Luo P, Yao W, Susmel L, Wang Y, Ma X. A survey on multiaxial fatigue damage parameters under non-proportional loadings. Fatigue Fract Eng Mater Struct 2017;40(9):1323–42.

[12] Wu ZR, Hu XT, Li ZX, Song YD. Evaluation of fatigue life for titanium alloy TC4 under variable amplitude multiaxial loading. Fatigue Fract Eng Mater Struct 2015;38(4):402–9.

[13] Wu ZR, Hu XT, Song YD. Multiaxial fatigue life prediction for titanium alloy TC4 under proportional and nonproportional loading. Int J Fatigue 2014;59:170–5.

[14] Yu ZY, Zhu SP, Liu Q, Liu Y. A new energy-critical plane damage parameter for multiaxial fatigue life prediction of turbine blades. Materials (Basel) 2017;10(5):513.

[15] Xu S, Zhu SP, Hao YZ, Liao D, Qian G. A new critical plane-energy model for multiaxial fatigue life prediction of turbine disc alloys. Eng Fail Anal 2018;93:55–63.

[16] Zhu SP, Yu ZY, Correia J, De Jesus A, Berto F. Evaluation and comparison of critical plane criteria for multiaxial fatigue analysis of ductile and brittle materials. Int J Fatigue 2018;112:279–88.

[17] Findley WN. A Theory for the Effect of Mean Stress on Fatigue of Metals Under Combined Torsion and Axial Load or Bending. J Eng Ind 1959;81(4):301–5.

[18] Karolczuk A, Macha. E. A review of critical plane orientations in multiaxial fatigue failure criteria of metallic materials. Int J Fract 2005;134(3–4):267–304.

[19] Carpinteri A, Spagnoli A, Vantadori S. A multiaxial fatigue criterion for random loading. Fatigue Fract Eng Mater Struct 2003;26(6):515–22.

[20] Wang CH, Brown MW. A path-independent parameter for fatigue under proportional and non-proportional loading. Fatigue Fract Eng Mater Struct 1993;16(12):1285–97.

[21] Fatemi A, Socie DF. A critical plane approach to multiaxial fatigue damage including out-of-phase loading. Fatigue Fract Eng Mater Struct 1988;11(3):149–65.

[22] Wang XW, Shang DG, Sun YJ. A weight function method for multiaxial low-cycle fatigue life

prediction under variable amplitude loading. J Strain Anal Eng Des 2018;53(4):197–209.

[23] Smith K.N, Watson P, Topper TH. A Stress- strain function for the fatigue of metals. J Mater 1970;5(4):767–78.

[24] Ince A, Glinka G. A generalized fatigue damage parameter for multiaxial fatigue life prediction under proportional and non-proportional loadings. Int J Fatigue 2014;62:34–41.

[25] Liu KC, Wang JA. An energy method for predicting fatigue life, crack orientation, and crack growth under multiaxial loading conditions. Int J Fatigue 2001;23:129–34.

[26] Varvani-Farahani A. New energy-critical plane parameter for fatigue life assessment of various metallic materials subjected to in-phase and out-of-phase multiaxial fatigue loading conditions. Int J Fatigue 2000;22(4):295–305.

[27] Bemfica C, Carneiro L, Mamiya EN, Castro FC. Fatigue and cyclic plasticity of 304L stainless steel under axial-torsional loading at room temperature. Int J Fatigue 2019;125:349–61.

[28] Noban M, Jahed H, Ibrahim E, Ince A. Load path sensitivity and fatigue life estimation of 30CrNiMo8HH. Int J Fatigue 2012;37:123–33.

[29] Rozumek D, Marciniak Z. Fatigue crack growth in AlCu4Mg1 under nonproportional bending-with-torsion loading. Mater Sci 2011;46(5):685–94.

[30] Liu Y, Mahadevan S. Strain-based multiaxial fatigue damage modelling. Fatigue Fract Eng Mater Struct 2005;28(12):1177–89.

[31] Kanazawa K, Miller KJ, Brown MW. Cyclic deformation of 1% Cr-Mo-V steel under out-of-phase loads. Fatigue Fract Eng Mater Struct 1979;2(2):217–28.

[32] Lu Y, Wu H, Zhong Z. A simple energy-based model for nonproportional low-cycle multiaxial fatigue life prediction under constant-amplitude loading. Fatigue Fract Eng Mater Struct 2018;41(6):1402–11.

[33] Shamsaei N, Fatemi A. Effect of microstructure and hardness on non-proportional cyclic hardening coefficient and predictions. Mater Sci Eng A 2010;527(12):3015–24.

[34] Borodii M V., Shukaev SM. Additional cyclic strain hardening and its relation to material structure, mechanical characteristics, and lifetime. Int J Fatigue 2007;29(6):1184–91.

[35] Anes V, Reis L, Li B, De Freitas M. New approach to evaluate non-proportionality in multiaxial loading conditions. Fatigue Fract Eng Mater Struct 2014;37(12):1338–54.

[36] Borodii M V., Strizhalo VA. Analysis of the experimental data on a low cycle fatigue under

nonproportional straining. Int J Fatigue 2000;22(4):275–82.

[37] Zhong B, Wang Y, Wei D, Wang J. A new life prediction model for multiaxial fatigue under proportional and non-proportional loading paths based on the pi-plane projection. Int J Fatigue 2017;102:241–51.

[38] Meggiolaro MA, De Castro JTP. An improved multiaxial rainflow algorithm for non-proportional stress or strain histories - Part I: Enclosing surface methods. Int J Fatigue 2012;42:217–26.

[39] Meggiolaro MA, De Castro JTP. Prediction of non-proportionality factors of multiaxial histories using the Moment of Inertia method. Int J Fatigue 2014;61:151–9.

[40] Meggiolaro MA, de Castro JTP, Wu H. On the use of tensor paths to estimate the nonproportionality factor of multiaxial stress or strain histories under free-surface conditions. Acta Mech 2016;227(11):3087–100.

[41] Kanazawa K, Miller KJ, Brown MW. Low-cycle fatigue under out-of-phase loading conditions. J Eng Mater Technol Trans ASME 1977;99(3):222–8.

[42] Li J, Li CW, Zhang ZP. Modeling of stable cyclic stress-strain responses under non-proportional loading. ZAMM Zeitschrift Fur Angew Math Und Mech 2018;98(3):388–411.

[43] Li J, Zhang Z ping, Li C wang. An improved Armstrong–Frederick-Type Plasticity Model for Stable Cyclic Stress–Strain Responses Considering Nonproportional Hardening. J Mater Eng Perform 2018;27(4):2038–48.

[44] Chen X, Gao Q, Sun XF. Low-cycle fatigue under non-proportional loading. Fatigue Fract Eng Mater Struct 1996;19(7):839–54.

[45] Bolchoun A, Kaufmann H, Sonsino CM. Numerical measures of the degree of non-proportionality of multiaxial fatigue loadings. Frat Ed Integrita Strutt 2015;9(33):238–52.

[46] Skibicki D, Sempruch J. Use of a load non-proportionality measure in fatigue under out-of-phase combined bending and torsion. Fatigue Fract Eng Mater Struct 2004;27(5):369–77.

[47] Nitta A, Ogata T, Kuwabara K. Fracture mechanisms and life assessment under high-strain biaxial cyclic loading of type 304 stainless steel. Fatigue Fract Eng Mater Struct 1989;12(2):77–92.

[48] Ma S, Markert B, Yuan H. Multiaxial fatigue life assessment of sintered porous iron under proportional and non-proportional loadings. Int J Fatigue 2017;97:214–26.

[49] Skibicki D, Pejkowski Ł. Low-cycle multiaxial fatigue behaviour and fatigue life prediction for CuZn37 brass using the stress-strain models. Int J Fatigue 2017;102:18–36.

[50] Fatemi A, Shamsaei N. Multiaxial fatigue: An overview and some approximation models for life estimation. Int J Fatigue 2011;33(8):948–58.

[51] Itoh T, Sakane M, Ohsuga K. Multiaxial low cycle fatigue life under non-proportional loading. Int J Press Vessel Pip 2013;110:50–6.

[52] Itoh T, Yang T. Material dependence of multiaxial low cycle fatigue lives under non-proportional loading. Int J Fatigue 2011;33(8):1025–31.

[53] Wang CH, Brown MW. Life prediction techniques for variable amplitude multiaxial fatigue—Part 1: Theories. J Eng Mater Technol 1996;118(3):367–70.

[54] Li J, Zhang ZP, Sun Q, Li CW. Multiaxial fatigue life prediction for various metallic materials based on the critical plane approach. Int J Fatigue 2011;33(2):90–101.

[55] Ellyin F, Xia Z. A general fatigue theory and its application to out-of-phase cyclic loading. J Eng Mater Technol Trans ASME 1993;115(4):411–6.

[56] Taira S, Inoue T, Yoshida T. Low cycle fatigue under multiaxial stresses: in the case of combined cyclic tension-compression and cyclic torsion at room temperature. Trans Japan Soc Mech Eng 1969;35(271):526–32.

[57] Lamba HS, Sidebottom OM. Cyclic plasticity for nonproportional paths: part 1 – cyclic hardening, erasure of memory, and subsequent strain hardening experiments. ASME J Eng Mater Technol 1978;100:96–103.

[58] Socie D. Multiaxial fatigue damage models. ASME J Eng Mater Technol 1987;109(4):293–8.

[59] Doong SH, Socie DF, Robertson IM. Dislocation substructures and nonproportional hardening. ASME J Eng Mater Technol 1990;112(4):456–64.

[60] Itoh T, Sakane M, Ohsuga K. Multiaxial low cycle fatigue life under non-proportional loading. Int J Press Vessel Pip 2013;110:50–6.

[61] de Freitas M, Reis L, Li B. Comparative study on biaxial low-cycle fatigue behaviour of three structural steels. Fatigue Fract Eng Mater Struct 2006;29(12):992–9.

[62] Tanaka E, Murakami S, Ooka M. Effects of strain path shapes on non-proportional cyclic plasticity. J Mech Phys Solids 1985;33(6):559–75.

[63] Itoh T, Sakane M, Ohnami M, Socie DF. Nonproportional low cycle fatigue criterion for type 304 stainless steel. J Eng Mater Technol Trans ASME 1995;117(3):285–92.

[64] Dong P, Wei Z, Hong JK. A path-dependent cycle counting method for variable-amplitude multi-

axial loading. Int J Fatigue 2010;32(4):720–34.

[65] Mei J, Dong P. A new path-dependent fatigue damage model for non-proportional multi-axial loading. Int J Fatigue 2016;90:210–21.

[66] Liu B, Yan X. A new method for studying the effect of multiaxial strain states on low cycle non-proportional fatigue prediction. Int J Fatigue 2018;117:420–31.

[67] Brown MW, Miller KJ. A Theory for Fatigue Failure under Multiaxial Stress-Strain Conditions. Proc Inst Mech Eng 1973;187(1):745–55.

[68] Yu ZY, Zhu SP, Liu Q, Liu YH. Multiaxial fatigue damage parameter and life prediction without any additional material constants. Materials (Basel) 2017;10(8):923.

[69] Itoh T, Nakata T, Sakane M, Ohnami M. Nonproportional low cycle fatigue of 6061aluminum alloy under 14 strain paths. Eur. Struct. Integr. Soc., vol. 25, 1999;, p. 41–54.

[70] Zhou H, Deng Z, Xia Y, Fu M. A new sampling method in particle filter based on Pearson correlation coefficient. Neurocomputing 2016;216:208–15.

[71] Lopez-Crespo P, Moreno B, Lopez-Moreno A, Zapatero J. Study of crack orientation and fatigue life prediction in biaxial fatigue with critical plane models. Eng Fract Mech 2015;136:115–30.

[72] Karolczuk A, Skibicki D, Pejkowski Ł. Evaluation of the Fatemi-Socie damage parameter for the fatigue life calculation with application of the Chaboche plasticity model. Fatigue Fract Eng Mater Struct 2019;42(1):197–208.

[73] Standard A. E2207–02. Standard practice for strain-controlled axial-torsional testing with thin walled tube specimens. Annu B ASTM Stand 2007;3:1297–304.

Title: Load path sensitivity and multiaxial fatigue life prediction of metals under non-proportional loadings

Highlights:

(1) A new definition of non-proportional degree on generalized plane for non-proportional loading;

(2) A new model without additional material constants for fatigue life assessment under non-proportional loadings;

(3) Experimental data of three materials under different loading paths verified model predictions accuracy.

Declaration of Interest Statement

The authors declared that they do not have any commercial or associative interest that represents a conflict of interest in connection with the work submitted, entitled "*Load path sensitivity and multiaxial fatigue life prediction of metals under non-proportional loadings*".